



Contents lists available at ScienceDirect

Journal of Organometallic Chemistry

journal homepage: www.elsevier.com/locate/jorganchemPhotochemistry of hybrid organic–inorganic triarylborane-*o*-carboranesSo-Yoen Kim^a, Ah-Rang Lee^b, Yang-Jin Cho^a, Ho-Jin Son^{a,*}, Won-Sik Han^{b,*}, Sang Ook Kang^{a,*}^a Department of Advanced Materials Chemistry, Korea University, Sejong 339-700, Republic of Korea^b Department of Chemistry, Seoul Women's University, Seoul 139-774, Republic of Korea

ARTICLE INFO

Article history:

Received 12 March 2015

Received in revised form

14 April 2015

Accepted 15 April 2015

Available online xxx

Keywords:

Carborane photochemistry

Intramolecular charge-transfer

Hybrid organic–inorganic boron complexes

ABSTRACT

Para- and *meta*-substituted *o*-carboranes with a dimesityl(phenyl)borane (dmpb) group, namely, **p-1**, **p-2**, **m-1**, and **m-2**, were prepared and their electronic natures were evaluated by steady-state photo-physical methods. It was found that excited states were greatly influenced by the linking position of the dimesityl-borane group(s) at the phenyl unit of diphenyl-*o*-carboranes. While intramolecular charge-transfer (ICT) prevails in both *para*- and *meta*-regioisomers, *para*-isomers show much enhanced ICT character, as evidenced by observation of a new emission band at $\lambda_{\text{max}} \approx 570$ nm in dichloromethane (DCM) solution. Furthermore, the solvatochromic shifts, $\Delta\nu_f$, from *n*-hexane to DCM were significantly different for *para*- and *meta*-isomers, which showed 8105, 8184, 1834, and 1895 cm^{-1} for **p-1**, **p-2**, **m-1**, and **m-2**, respectively. The difference in dipole moment between ground and excited states for *para*- (~31.8 D) and *meta*-isomers (~15.0 D) by using Mataga–Lippert plot confirmed that the ICT occurs from dimesityl-borane to *o*-carborane in *para*-isomers while the ICT occurs only from dimesityl-borane to the bridged phenyl group in *meta*-isomers. Excited state estimation by electrochemical and DFT studies corroborated well to the ICT character, and even with engagement of the strong electron withdrawing dimesityl-borane group *o*-carborane unit still acts as an electron acceptor as found in the *para*-isomers, **p-1** and **p-2**.

© 2015 Elsevier B.V. All rights reserved.

Introduction

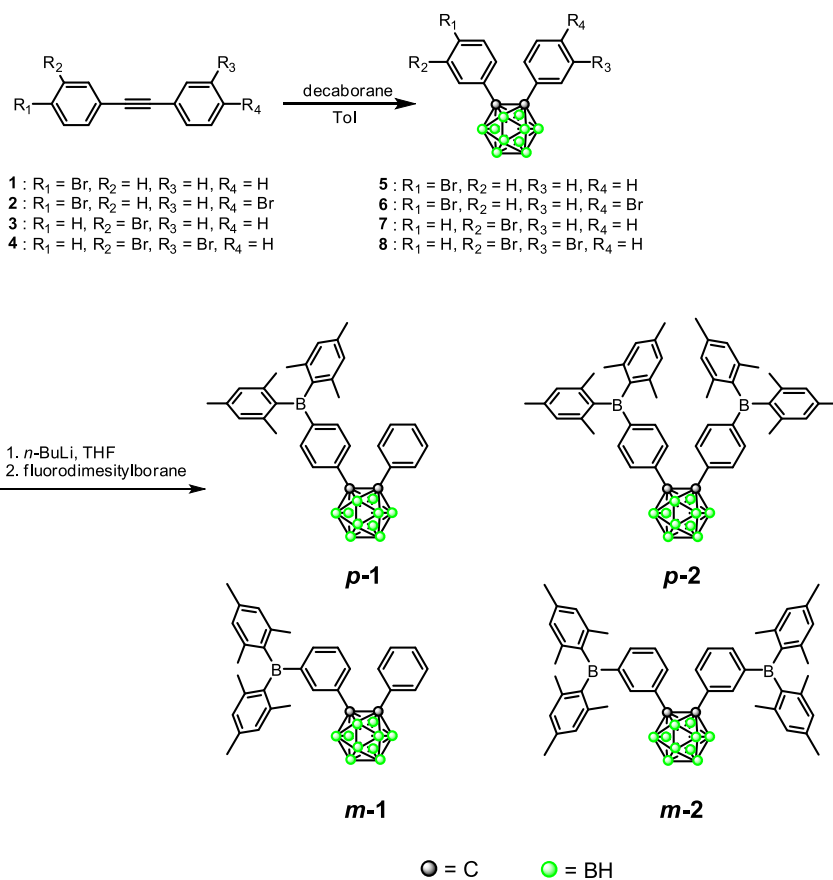
Tri-coordinated organoborane with its electron deficient nature of the central boron atom, is an important electron-acceptor for π -conjugated materials and has drawn much attention as potential organic electronic materials applicable to blue-light fluorescence, anion sensing, and nonlinear optics [1]. One way to stabilize an electron deficient boron atom is to replenish electrons to the central boron through the π -electron channels from neighboring organic functional groups. In most cases, organic functional groups were aryl or alkylated aryl groups facilitating $p_{\pi} \rightarrow p_{\pi}^*$ orbital interaction from aryl groups to the boron atom [2–4]. Depending on the electron donating power of the aryl substituent, much enhanced π -type interaction was foreseeable. When strong electron donating (ED) amine groups were engaged to the π -aryls,

distinctive electron donor–acceptor dyads were formed to show a low energy charge-transfer (CT) transition band in their photoluminescent spectra [5].

Within the context of further exploration of potential photo-functional materials in the realms of organoboranes, electron deficient inorganic cluster boranes are introduced in this work. Recently, *o*-carborane derivatives have shown to be efficient π -electron acceptors if they were coordinated to the aryl groups [6]. Even though the nature of the π -electron acceptor character between organoboranes and *o*-carboranes differs greatly, combination of these two units into a single molecule would create new types of hybrid organic–inorganic boron complexes otherwise unable to predict their electronic nature. In this regard, incorporation of *o*-carboane and triarylborane has been reported as a fluoride ion sensor [7], but their detailed photophysical properties were not reported. To establish further structure–electronic property relationship, we have prepared a series of triarylborane-*o*-carboranes in which dimesitylboranes were attached to the *para*- and *meta*-position of diphenyl-*o*-carborane, as shown in Scheme 1. It has been found that incorporation of organoboranes into the

* Corresponding authors.

E-mail addresses: hjson@korea.ac.kr (H.-J. Son), wshan@swu.ac.kr (W.-S. Han), sangok@korea.ac.kr (S.O. Kang).

Scheme 1. Synthetic routes for **p-1**, **p-2**, **m-1**, and **m-2**.

inorganic boron cluster produced a new type of electron acceptor featuring extended electronic conjugation between organic and inorganic boranes. Among the series, the *para*-isomers showed notable π -electronic communication between dimesityl-borane and *o*-carborane through the phenyl bridge. Steady-state photochemistry of the *para*-isomers revealed that intramolecular charge-transfer (ICT) process was a dominant feature found in polar organic solvents.

Experimental section

General procedures

All manipulations were carried out under a dry nitrogen or argon atmosphere using standard Schlenk techniques. THF was distilled freshly over sodium benzophenone. The ¹H, ¹¹B, and ¹³C NMR spectra were recorded on a Varian Mercury 300 spectrometer operating at 300.1, 96.3, and 75.4 MHz, respectively. All proton and carbon chemical shifts were measured relative to the internal residual benzene from the lock solvent (99.5% CDCl₃). ¹¹B NMR chemical shifts were referenced to BF₃·O(C₂H₅)₂ (0.0 ppm), with a negative sign indicating an up-field shift. The elemental analyses were performed using a Carlo Erba Instruments CHNSO EA 1108 analyzer. High Resolution Tandem Mass Spectrometry (Jeol LTD JMS-HX 110/110A) was performed by the Korean Basic Science Institute. Cyclic voltammetry (CV) was performed in an electrolyte containing 1 mM of the electro-active compounds and 0.1 M tetrabutylammonium hexafluorophosphate (NBu₄PF₆) at room temperature under a N₂ atmosphere using a BAS 100B electrochemical analyzer. Glassy carbon, platinum wire, and

Ag|AgNO₃ (0.1 M) were used as the working, counter, and reference electrodes, respectively. All potentials were calibrated to the ferrocene/ferrocenium (Fc|Fc⁺) redox couple. Dimesitylborane fluoride and *n*-BuLi (2.5 M solution in *n*-hexanes) were purchased from Aldrich and used as obtained without any further purification. Decarborane (B₁₀H₁₄) was purchased from Katchem and used after sublimation. 1-bromo-4-(phenylethynyl)benzene (**1**), 1,2-bis(4-bromophenyl)ethyne (**2**), 1-bromo-3-(phenylethynyl)benzene (**3**), and 1,2-bis(3-bromophenyl)ethyne (**4**) were synthesized according to the literature procedure [8]. 1-bromo-4-(*o*-carboranyl)benzene (**5**) and **p-1**^a, 1,2-bis(4-bromophenyl)-*o*-carborane (**6**)^b were also prepared according to the literature procedure.

Synthesis of 1-bromo-3-(*o*-carboranyl)benzene (**7**)

The mixture of compound **3** (0.38 g, 1.50 mmol) and decarborane (0.21 g, 1.73 mmol) was dissolved in dry toluene (15 mL) at room temperature under N₂ atmosphere. *N,N*-Dimethylaniline (0.34 mL, 2.70 mmol) was added, and the mixture was refluxed for 5 h. After cooling to room temperature, the solvent was separated from the solid and evaporated. The residue was subjected to silica gel column chromatography with hexane as an eluent (*R*_f = 0.56). Recrystallization from chloroform and ethanol provided compound **7** as a colorless crystal (0.34 g, 0.92 mmol, 61%). ¹H NMR (CDCl₃): δ 7.56 (t, *J* = 2.1 Hz, 1H, Ar-*H*), 7.44 (m, 2H, Ar-*H*), 7.35 (m, 2H, Ar-*H*), 7.24 (m, 1H, Ar-*H*), 7.18 (m, 2H, Ar-*H*), 7.00 (t, *J* = 8.1 Hz, 1H), 1.50–3.70 (br, 10H, CB-BH). The ESI-MS calculated for C₁₄H₁₉B₁₀Br was 376.1601. Found: 377.2872 [M + H]⁺. Calcd for C₁₄H₁₉B₁₀Br: C, 44.80; H, 5.10. Found: C, 44.75; H, 5.09.

Synthesis of 1,2-bis(3-bromophenyl)-o-carborane (**8**)

The compound was synthesized according to a procedure similar to that for **7**, using **4** (0.50 g, 1.50 mmol) instead of **3** to give colorless crystal (0.46 g, 1.01 mmol, 67%). ^1H NMR (CDCl_3): δ 7.58 (t, $J = 2.1$ Hz, 2H, Ar–H), 7.38 (m, 4H, Ar–H), 7.06 (t, $J = 8.1$ Hz, 2H, Ar–H), 1.50–3.70 (br, 10H, CB–BH). The ESI-MS calculated for $\text{C}_{14}\text{H}_{18}\text{B}_{10}\text{Br}_2$ was 454.0706. Found: 455.0536 $[\text{M} + \text{H}]^+$. Calcd for $\text{C}_{14}\text{H}_{18}\text{B}_{10}\text{Br}_2$: 37.02; H, 3.99. Found: C, 37.04; H, 4.00.

Synthesis of 1,2-bis(4-(Dimesitylboryl)phenyl)-o-carborane (**p-2**)

A hexane solution of *n*-BuLi (2.5 M, 0.56 mL, 1.39 mmol) was added at -78 °C to a solution of **6** (0.29 g, 0.63 mmol) in THF (20 mL), and the mixture was stirred for 1 h at that temperature. A solution of dimesitylboron fluoride (0.41 g, 90%, 1.39 mmol) in THF (20 mL) was added to the mixture. The reaction mixture was stirred for 1 h at -78 °C, allowed to slowly warm to room temperature, and stirred overnight. After quenching by saturated aqueous NH_4Cl (30 mL), the aqueous layer was extracted further with dichloromethane. The combined organic layers were washed with water (3×30 mL), dried over MgSO_4 , and concentrated under reduced pressure. The residue was suspended with a EtOAc/MeOH mixed solvent. The insoluble part was collected by filtration and washed with MeOH to afford the desired product **p-2** as a white solid (0.24 g, 48%). ^1H NMR (CDCl_3): δ 7.33 (d, $J = 8.4$ Hz, 4H, $\text{Mes}_2\text{B}-\text{Ph}-\text{CH}$), 7.21 (d, $J = 7.8$ Hz, 4H, $\text{Ph}-\text{CH}$), 6.77 (s, 8H, $\text{Mes}-\text{CH}$), 2.29 (s, 12H, $\text{Mes}-\text{CH}_3$), 1.84 (s, 24H, $\text{Mes}-\text{CH}_3$), 1.50–3.70 (br, 10H, CB–BH). ^{13}C NMR (CDCl_3): δ 147.98, 141.42, 140.83, 139.39, 135.67, 133.65, 130.22, 128.51, 127.11, 84.87, 23.59, 21.44. ^{11}B NMR (CDCl_3): δ -0.44 , -8.13 . The ESI-MS calculated for $\text{C}_{50}\text{H}_{62}\text{B}_{12}$ was 794.5968. Found: 795.4572 $[\text{M} + \text{H}]^+$. Calcd for $\text{C}_{50}\text{H}_{62}\text{B}_{12}$: C, 89.02; H, 7.77; B, 3.21. Found: C, 89.01; H, 7.78.

Synthesis of dimesityl(3-(o-carboranyl)phenyl)borane (**m-1**)

The compound was synthesized according to a procedure similar to that for **p-2**, using **7** (0.35 g, 0.92 mmol) instead of **6** with *n*-BuLi (2.5 M, 0.40 mL, 1.01 mmol) and dimesitylboron fluoride (0.30 g, 90%, 1.01 mmol) to give 0.26 g of white powder (52% yield). ^1H NMR (CDCl_3): δ 7.60 (d, $J = 7.5$ Hz, 1H, $\text{Mes}_2\text{B}-\text{Ph}-\text{CH}$), 7.35 (m, 3H, $\text{Mes}_2\text{B}-\text{Ph}-\text{CH}$), 7.42 (s, 1H, $\text{Mes}_2\text{B}-\text{Ph}-\text{CH}$), 7.24–7.07 (m, 4H, $\text{Ph}-\text{CH}$), 6.79 (s, 4H, $\text{Mes}-\text{CH}$), 2.32 (s, 6H, $\text{Mes}-\text{CH}_3$), 1.78 (s, 12H, $\text{Mes}-\text{CH}_3$), 1.50–3.70 (br, 10H, CB–BH). ^{13}C NMR (CDCl_3): δ 146.37, 141.18, 140.82, 139.34, 137.75, 137.69, 134.02, 130.86, 130.45, 130.24, 128.51, 128.46, 128.29, 85.36, 85.22, 23.53, 21.49. ^{11}B NMR (CDCl_3): δ -0.76 , -8.73 . The ESI-MS calculated for $\text{C}_{32}\text{H}_{41}\text{B}_{11}$ was 546.4232. Found: 546.9825 $[\text{M}]^+$. Calcd for $\text{C}_{32}\text{H}_{41}\text{B}_{11}$: C, 70.57; H, 7.59; B, 21.84. Found: C, 70.55; H, 7.60.

Synthesis of 1,2-bis(3-(Dimesitylboryl)phenyl)-o-carborane (**m-2**)

The compound was synthesized according to a procedure similar to that for **p-1**, using **8** (0.29 g, 0.63 mmol) instead of **6** with *n*-BuLi (2.5 M, 0.56 mL, 1.39 mmol) and dimesitylboron fluoride (0.41 g, 90%, 1.39 mmol) to give 0.21 g of white powder (43% yield). ^1H NMR (CDCl_3): δ 7.56 (s, 2H, $\text{Mes}_2\text{B}-\text{Ph}-\text{CH}$), 7.43 (d, $J = 7.8$ Hz, 2H, $\text{Mes}_2\text{B}-\text{Ph}-\text{CH}$), 7.35 (d, $J = 7.8$ Hz, 2H, $\text{Mes}_2\text{B}-\text{Ph}-\text{CH}$), 7.10 (t, $J = 7.8$ Hz, 2H, $\text{Ph}-\text{CH}$), 6.80 (s, 8H, $\text{Mes}-\text{CH}$), 2.32 (s, 12H, $\text{Mes}-\text{CH}_3$), 1.80 (s, 24H, $\text{Mes}-\text{CH}_3$), 1.50–3.70 (br, 10H, CB–BH). ^{13}C NMR (CDCl_3): δ 146.27, 141.17, 140.84, 139.40, 138.61, 137.89, 133.91, 130.57, 128.56, 128.22, 85.60, 23.60, 21.49. ^{11}B NMR (CDCl_3): δ -0.53 , -8.61 . The ESI-MS calculated for $\text{C}_{50}\text{H}_{62}\text{B}_{12}$ was 794.5968.

Found: 795.2367 $[\text{M} + \text{H}]^+$. Calcd for $\text{C}_{50}\text{H}_{62}\text{B}_{12}$: C, 89.02; H, 7.77; B, 3.21. Found: C, 89.00; H, 7.76.

Crystal structure determination

Single crystals of **p-2**, **m-1**, and **m-2** were sealed in glass capillaries under argon and mounted a diffractometer. The preliminary examination and data collection were performed on a Bruker SMART CCD detector system single-crystal X-ray diffractometer equipped with a sealed-tube X-ray source (50 kV \times 30 mA) using graphite-monochromated Mo K_α radiation ($\lambda = 0.71073$ Å). The preliminary unit cell constants were determined using a set of 45 narrow-frame (0.3° in ω) scans. A double-pass method of scanning was used to exclude any noise. The collected frames were integrated using an orientation matrix determined from the narrow-frame scans. The SMART software package was used for data collection and SAINT was used for frame integration [9]. Final cell constants were determined by a global refinement of the xyz centroids of the reflections harvested from the entire data set. Structure solution and refinement were carried out using the SHELXTL-PLUS software package [10].

Absorption and emission spectra

The absorption and photoluminescence spectra were recorded on an SHIMADZU UV-3101PC UV–VIS–NIR scanning spectrophotometer and a VARIAN Cary Eclipse fluorescence spectrophotometer, respectively.

Thermal property

Thermal properties were measured using differential scanning calorimetry (Perkin–Elmer/Pyris Diamond DSC). A heating rate of 10 °C/min was used after first melting the compound, followed by a rapid cooling rate of 40 °C/min to room temperature.

DFT calculations

Theoretical calculations for the derivatives were conducted on the Gaussian 09 package [11]. The ground-state geometries of **p-1**, **p-2**, **m-1**, and **m-2** were optimized by using the B3LYP density functional theory (DFT) and 6–31G(d,p) basis set. Time-dependent DFT (TDDFT) calculations were then performed with the same functional and basis set to estimate the energies and oscillator strengths of the derivatives. The contours of the electron density were plotted by using Chem3D ver.10.

Results and discussion

Synthesis and structure characterization

A series of *para*- and *meta*-regioisomers, **p-1**, **p-2**, **m-1**, and **m-2**, were prepared in modest yields by the reaction between the lithium salts derived from 1-bromo-*x*-(*o*-carboranyl)benzene ($x = 4$ for **5** and 3 for **7**), 1,2-bis(*x*-bromophenyl)-*o*-carborane ($x = 4$ for **6** and 3 for **8**) and fluorodimesitylborane, as shown in Scheme 1. Except **p-1**, the single crystals of **p-2**, **m-1**, and **m-2** were grown from a dichloro-methane/*n*-hexane mixed solution and their crystal structures are shown in Fig. 1. The single crystal structure for **p-1** was reported previously [7a]. Selected crystal data are summarized in Table 1 and full crystal data with collection parameters are in Table S1 in the supporting data. Among the crystal structures, **p-2** was crystallized in the orthorhombic crystal system with *Pbcn* space group while **m-1** and **m-2** were crystallized in the triclinic crystal system with *P-1* space group. The adjacent phenyl rings to *o*-

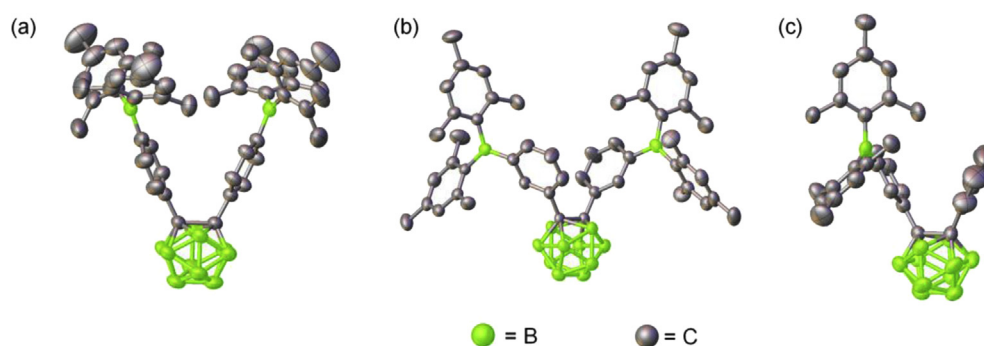


Fig. 1. Single crystal structures of **p-2** (a), **m-1** (b), and **m-2** (c) with 50% thermal ellipsoid. The hydrogen atoms are omitted for clarity.

carborane are disposed orthogonally to the C–C bond of the carborane cage with dihedral angles of $71.6(2)^\circ$, $75.0(1)^\circ$, and $85.8(2)^\circ$ for **p-2**, **m-1**, and **m-2**, respectively. The C–C bond distance of *o*-carborane cages ($1.721(3)$ Å for **p-2**, $1.725(2)$ Å for **m-1**, and $1.728(3)$ Å for **m-2**) were significantly longer than that of the nonsubstituted *o*-carborane (1.629 Å) [12] which indicates electron-withdrawing (EW) character of **p-2**, **m-1**, and **m-2** because it is known that the C–C bond distance in carborane cage is elongated when *o*-carborane accepts one-electron [13].

Photophysical properties

Fig. 2 shows the electronic absorption and fluorescence spectra of **p-1**, **p-2**, **m-1**, and **m-2** in dichloromethane (DCM) solution and their spectroscopic data are summarized in Table 2. All of the prepared compounds exhibited similar absorption spectra with two main absorption bands in the range of 250–365 nm and the spectra were characterized by broad lowest energy and relatively structured higher energy absorption bands. The higher energy absorption band observed for each compound can be ascribed to the $\pi-\pi^*$ transition of the aryl group [14]. The lowest energy absorption bands of each compound are assigned to CT transitions between p orbitals of the aryl group, p(aryl), and vacant p orbitals of the central boron atom, p(B). The extinction coefficients (ϵ) of **p-2** and **m-2** with two dimesityl(phenyl)borane (dmpb) units are approximately double those with one dmpb unit in **p-1** and **m-1**, as summarized in Table 2. Also, all compounds showed close similarities of the absorption energy and spectral band shapes with the dmpb. These results indicate that all compounds have negligible electronic coupling between dmpb and *o*-carborane moieties in the ground state. Therefore, the boron atom in the dmpb groups for all compounds act as an electron acceptor, while the *o*-carborane group is simply a spectator in the ground state.

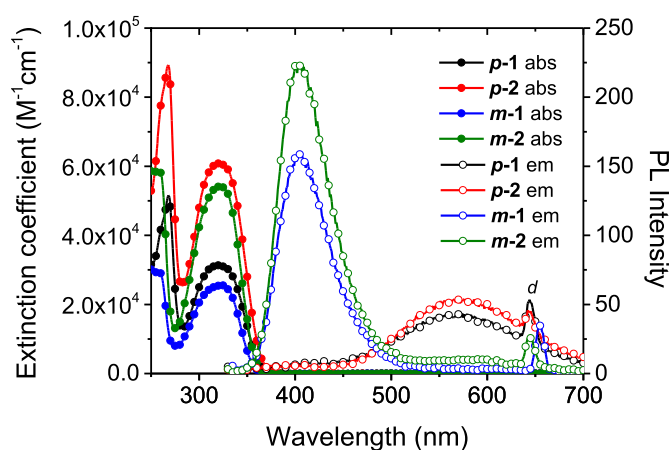


Fig. 2. UV/Vis absorption and fluorescence spectra of dimesityl(phenyl)borane-*o*-carboranes, **p-1**, **p-2**, **m-1**, and **m-2**, for 10 μM solution in dichloromethane (DCM).

In the fluorescence spectra, on the other hand, *para*- and *meta*-regioisomers showed significantly different behaviors. In general, the fluorescence of triarylborane derivatives comes from p(aryl)–p(B) CT excited states which is evidenced by fluoride-addition experiments [3]. For *meta*-isomers, typical emission from p(aryl)–p(B) CT excited states were observed at $\lambda_{\text{max}} \approx 400$ nm in DCM solution. In contrast to *meta*-isomers, *para*-isomers showed a broad emission band at $\lambda_{\text{max}} \approx 570$ nm along with relatively weak emission intensity, as shown in Fig. 2. It should be noted that the emission from p(aryl)–p(B) CT excited states disappeared and only the new emission band was observed. This broad red-shifted emission can be attributed to the strong intramolecular charge-transfer (ICT) state derived from the presence of *o*-carborane group at the *para*-position, as shown by the remarkable

Table 1
Summary of crystal data for **p-2**, **m-1**, and **m-2**.

Identification code	p-2	m-1	m-2
Empirical formula	$\text{C}_{50}\text{H}_{62}\text{B}_{12}$	$\text{C}_{32}\text{H}_{41}\text{B}_{11}$	$\text{C}_{50}\text{H}_{62}\text{B}_{12}$
Formula weight	792.71	544.56	792.71
Wavelength	0.71073 Å	0.71073 Å	0.71073 Å
Crystal system, space group	Orthorhombic, <i>Pbcn</i>	Triclinic, <i>P-1</i>	Triclinic, <i>P-1</i>
Unit cell dimensions	$a = 30.290(4)$ Å $b = 12.4277(15)$ Å $c = 26.818(3)$ Å	$a = 10.914(2)$ Å $\alpha = 94.359(4)^\circ$ $b = 11.236(2)$ Å $\beta = 94.151(4)^\circ$ $c = 27.191(5)$ Å $\gamma = 90.688(4)^\circ$	$a = 12.174(3)$ Å $\alpha = 66.980(4)^\circ$ $b = 14.430(3)$ Å $\beta = 84.020(5)^\circ$ $c = 15.288(3)$ Å $\gamma = 88.816(5)^\circ$
Volume	$10095(2)$ Å ³	$3315.4(11)$ Å ³	$2457.7(9)$ Å ³
Final R indices [$I > 2\sigma(I)$]	$R_1 = 0.0668$, ^a $wR_2 = 0.1637$ ^b	$R_1 = 0.0572$, ^a $wR_2 = 0.1561$ ^b	$R_1 = 0.0652$, ^a $wR_2 = 0.1699$ ^b
R indices (all data)	$R_1 = 0.1586$, ^a $wR_2 = 0.2385$ ^b	$R_1 = 0.1396$, ^a $wR_2 = 0.2076$ ^b	$R_1 = 0.1474$, ^a $wR_2 = 0.2258$ ^b

^a $R_1 = \sum ||F_o| - |F_c|| / \sum |F_o|$ (based on reflections with $F_o^2 > 2\sigma F^2$).

^b $wR_2 = [\sum [w(F_o^2 - F_c^2)^2] / \sum [w(F_o^2)^2]]^{1/2}$; $w = 1/[\sigma^2(F_o^2) + (0.095P)^2]$; $P = [\max(F_o^2, 0) + 2F_c^2]/3$ (also with $F_o^2 > 2\sigma F^2$).

Table 2
Optical, photophysical, and thermal properties of the compounds in DCM.

Comp.	Abs. λ_{\max} (nm), (ϵ , $M^{-1}cm^{-1}$)	Em. λ_{\max} (nm)	Stokes shift (cm^{-1})	E_{red} (V) ^a	E_{HOMO} (eV) ^a	E_{LUMO} (eV) ^b	T_g ($^{\circ}C$)
p-1	268 (51600), 321 (31400)	566	13,485	-1.67	-6.47	-3.13	83
p-2	268 (89300), 322 (60900)	575	13,665	-1.65	-6.46	-3.15	130
m-1	260 (29000), 323 (25500)	405	6268	-1.75	-6.46	-3.05	68
m-2	260 (58400), 322 (54200)	406	6425	-1.80	-6.36	-3.00	109

The HOMO and LUMO levels were determined using the following equations: ^a E_{HOMO} (eV) = $-e(E_{LUMO} - E_g^{opt})$, ^b E_{LUMO} (eV) = $-e(E_{onset}^{red} + 4.8)$.

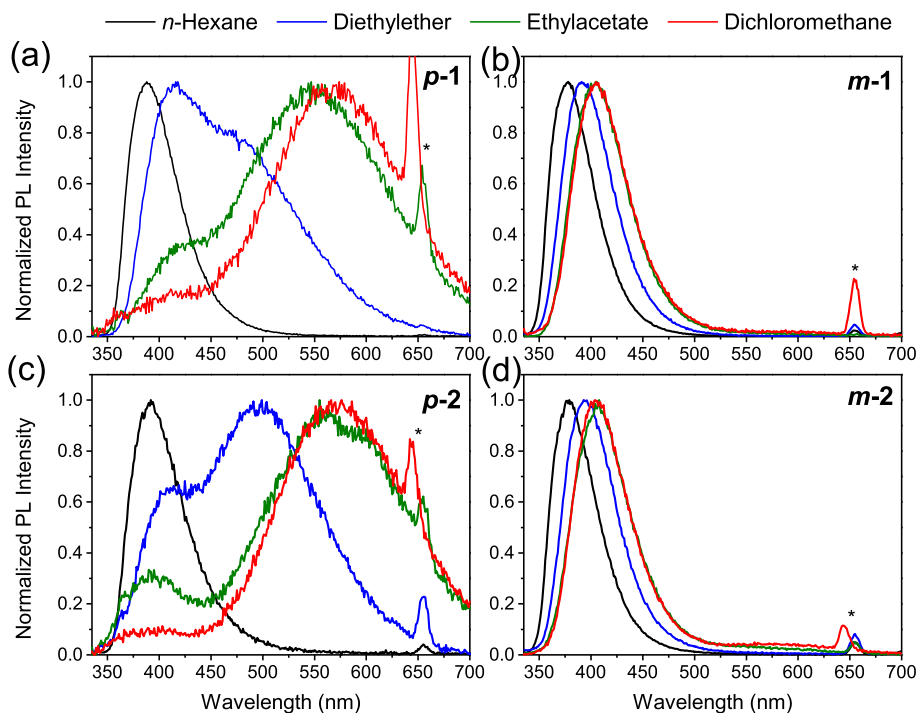


Fig. 3. Solvent dependent fluorescent spectra of **p-1** (a), **p-2** (b), **m-1** (c), and **m-2** (d). The fluorescence intensities are normalized to those at the maximum energies. Asterisk mark indicates the second order peak of the excitation wavelength at 322 or 327 nm.

solvatochromic shifts of the emission which depicted in Fig. 3. The fluorescence maximum energies of the derivatives (ν_f) shifted to lower energy as the solvent polarity increased. Such solvent effects have been observed for an ICT-type compound and are due to stabilization of the fluorescent ICT excited-state energy. In the present case, the solvatochromic shift of ν_f from *n*-hexane to DCM, $\Delta\nu_f$, was dependent on the nature of the regioisomer structure, as shown in Fig. 3 and Table 3. Mataga and Lippert showed that the solvent sensitivity to polarity can be analyzed in terms of difference in the dipole moments in the ground and excited states [15]. Thus, the difference in dipole moment between ground and excited states were measured for *para*- and *meta*-regioisomers by using a Mataga–Lippert plot which is essentially a plot of the Stokes shift of the fluorescence emission versus the solvent

polarity. As can be seen in Fig. 4, the Stokes shift of *para*-isomers changes linearly in response to the solvent polarity, which correlates highly with an increase in the dipole moments ($\Delta\mu$) of 31.80 and 31.77 D for **p-1** and **p-2**, respectively. On the other hand, *meta*-isomers showed much smaller dipole moments of 14.87 and 15.00 D for **m-1** and **m-2**, respectively. When one electron transfers the distance of 1 Å, the change of the dipole moment is 4.8 D. Therefore, observed dipole moment changes in *para*-isomers indicate that one-electron (unit charge) transfers the distance of ~6.6 Å, which corresponds to the distance between the dimesityl-donor and the carborane-acceptor. For *meta*-isomers, one-electron transfers the distance of ~3.1 Å, the equivalent distance between the dimesityl group and the bridged phenyl group. Therefore, we can conclude that *para*- and *meta*-regioisomers

Table 3
Solvent parameters and spectroscopic properties of **p-1**, **p-2**, **m-1**, and **m-2** in various solvents.

Solvent	Solvent parameter		p-1	p-2	m-1	m-2
	D_s	n	λ_{em} (nm/ cm^{-1})			
<i>n</i> -Hexane	1.904	1.3749	388/25773	391/25575	377/26525	377/26525
Diethylether	4.19	1.3527	483/20704	498/20080	391/25575	396/25253
Ethyl acetate	6.11	1.3724	547/18282	560/17857	401/24938	402/24876
Dichloromethane	9.14	1.4246	566/17668	575/17391	405/24691	406/24630
$\Delta\nu_f^a$			178/8105	184/8184	28/1834	29/1895

^a From *n*-hexane to DCM.

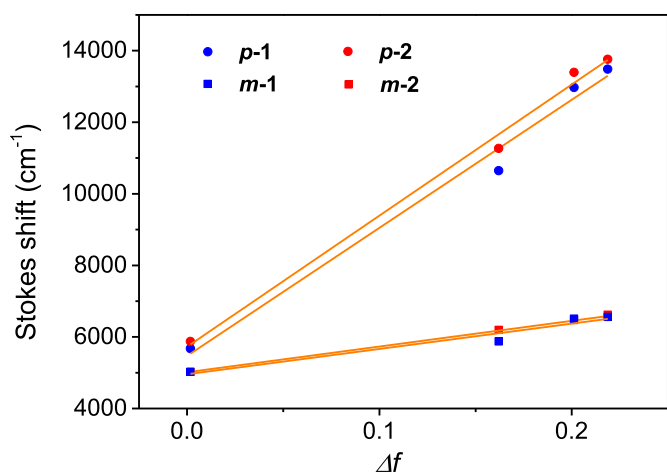


Fig. 4. Mataga–Lippert plots for **p-1**, **p-2**, **m-1**, and **m-2**. Increases in the dipole moments ($\Delta\mu$) are 31.80, 31.77, 14.87, and 15.16 D for **p-1**, **p-2**, **m-1**, and **m-2**, respectively.

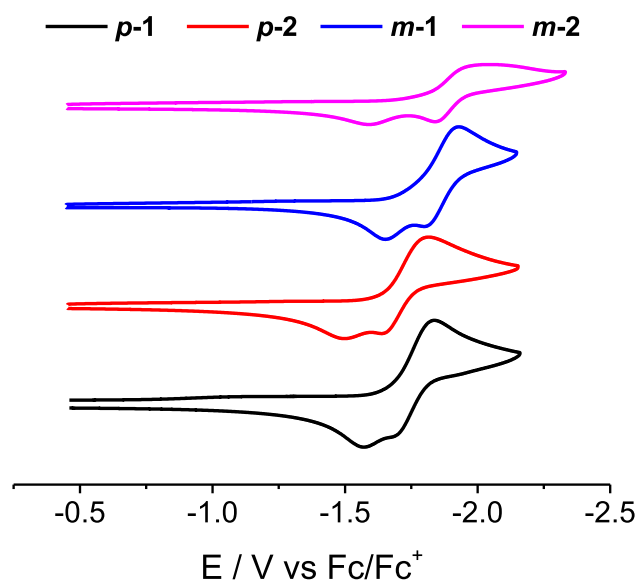


Fig. 5. Cyclic voltammograms for 0.1 mM DCM solution of **p-1**, **p-2**, **m-1**, and **m-2** containing 0.1 M TBAP taken at a scan rate of 0.1 V/s. Glassy carbon electrode is the working electrode, and a platinum wire and Ag/AgNO₃ is the counter and reference electrodes, respectively.

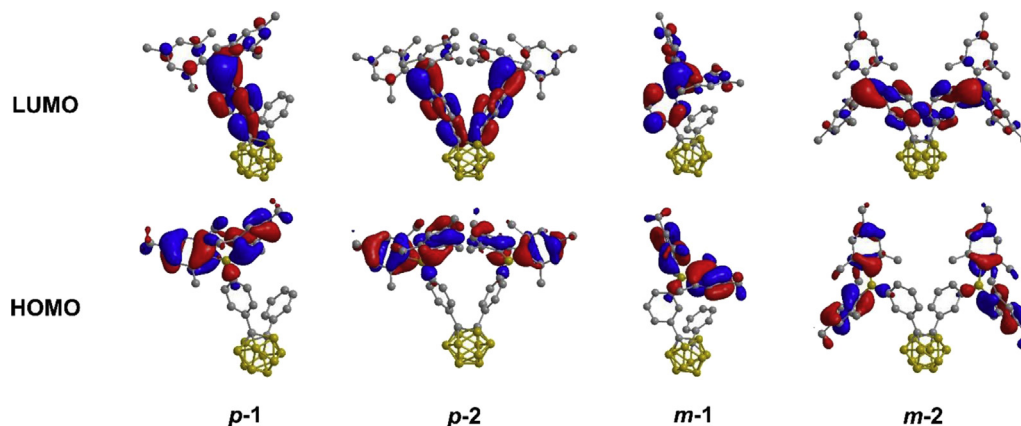


Fig. 6. Spatial distributions for the frontier orbitals of **p-1**, **p-2**, **m-1**, and **m-2**.

have completely different excited states and *o*-carborane in *para*-isomers only acts as a strong electron-accepting (EA) group, thereby opening the channel for electronic communication from dmpb to *o*-carborane.

Electrochemical properties

To confirm the different electronic states of the regioisomers, the electrochemical properties were investigated by using cyclic voltammogram (CV); their spectra are shown in Fig. 5 and the reduction potentials are summarized in Table 2. The reduction waves ($E_{\text{onset}}^{\text{red}}$) for **p-1** and **p-2** are observed at -1.67 and -1.65 V (versus Fc/Fc⁺), respectively. On the other hand, **m-1** and **m-2** showed their reduction waves ($E_{\text{onset}}^{\text{red}}$) at -1.75 and -1.80 V, respectively, slightly shifted to negative potential. The LUMO levels were determined by the following equation; E_{LUMO} (eV) = $-e(E_{\text{onset}}^{\text{red}} + 4.8)$. The calculated LUMO levels of *para*-isomers (-3.13 eV for **p-1** and -3.15 eV for **p-2**) are considerably lower than those of *meta*-isomers (-3.05 eV for **m-1** and -3.00 eV for **m-2**). Such a trend is in good agreement with emission property in which only *para*-isomers allow electronic communication between dmpb and the *o*-carborane unit.

Theoretical calculations

To gain insight into the electronic states of **p-1**, **p-2**, **m-1**, and **m-2**, DFT calculations were carried out using the B3LYP/6-31G(d,p) method with the Gaussian 09 package [11]. As shown in Fig. 6, all compounds showed that their HOMOs are mainly localized at the mesityl groups in the dmpb unit. On the other hand, distributions of LUMOs for *para*- and *meta*-regioisomers are significantly different. LUMOs of *para*-isomers are delocalized from the vacant p orbital on the boron atom to the *o*-carborane whereas LUMOs of *meta*-isomers are primarily localized at the vacant p orbital on the boron atom with little participation of phenyl units. Similar to results obtained from optical and electrochemical experiments, the LUMO levels (obtained by DFT calculation) of *para*-isomers are found to be substantially lower than those of *meta*-isomers: the LUMO levels of **p-1**, **p-2**, **m-1**, and **m-2** are -2.10 , -2.15 , -1.93 , and -1.99 eV, respectively. The difference of the calculated HOMO levels were relatively small, depending on the position of dimesitylborane to diphenyl-*o*-carborane (-6.18 eV for **p-1** and **p-2**, -6.15 eV for **p-1** and **p-2**). Furthermore, time-dependent DFT (TD-DFT) calculations with the same functional and basis set confirm that the lowest-energy absorption transitions are mainly associated with the HOMO \rightarrow LUMO transition. The calculated five lowest-energy

absorption transitions of the compounds are summarized in Tables S2–S5 (in Supporting Information). This, again, shows the ICT transition occurring from dmpb group(s) to *o*-carborane is significantly effective in para-isomers but, for *meta*-isomer, such transition is nominal, the bent posture (*meta*-geometry) disfavoring the electronic communication between dmpb group(s) and *o*-carborane.

Conclusions

A series of hybrid molecules that bring organoborane dmpb units to the cluster *o*-carborane network have been prepared and their photophysical properties were carefully studied by means of the substitution position of the organoboranes. *para*-Isomers, **p-1** and **p-2**, produce a symmetrical organoborane assembly to the *o*-carborane allowing maximum π -conjugation whereas *meta*-isomers, **m-1** and **m-2**, create a bent posture that disrupts favorable π -interaction. With those geometrical variations, a marked photophysical difference was noted between *para*- and *meta*-isomers and an ICT process prevailed for the *p*-isomers, **p-1** and **p-2**. From this study, *o*-carborane was found to be an efficient electron acceptor when it was properly aligned to the π -channel even in the presence of a strong π -acceptor, dmpb unit.

Acknowledgments

This work was supported by Chungcheong institute for regional program evaluation(CIRPE) promotion project of the MOTIE (Ministry of Trade, Industry and Energy) Republic of Korea (Grant A0046 00226), the Materials/Components Technology Development Program (10042682) funded by the Ministry of Trade, industry & Energy (MI, Korea), the Industrial Core Technology Development Program (10044876) funded by the Ministry of Trade, industry & Energy (MI, Korea), and Basic Science Research Program through the National Research Foundation of Korea (NRF) funded by the Ministry of Education (NRF-2014R1A6A1030732).

Appendix A. Supplementary material

CCDC 1053275 (**p-2**), 105327 (**m-1**), and 1053274 (**m-2**) contain the supplementary crystallographic data for this paper. These data can be obtained free of charge from The Cambridge Crystallographic Data Centre via www.ccdc.cam.ac.uk/data_request/cif.

Appendix B. Supplementary data

Supplementary data related to this article can be found at <http://dx.doi.org/10.1016/j.jorganchem.2015.04.025>.

References

- Reviews:a) C.D. Entwistle, T.B. Marder, Chem. Mater. 16 (2004) 4574–4585;
b) S. Yamaguchi, A. Wakamiya, Pure Appl. Chem. 78 (2006) 1413–1424;
c) Z.M. Hudson, S. Wang, Acc. Chem. Res. 42 (2009) 1584–1596;
d) C.R. Wade, A.E.J. Broomsgrove, S. Aldridge, F.P. Gabbaï, Chem. Rev. 110 (2010) 3958–3984.
- a) T. Noda, Y. Shirota, J. Am. Chem. Soc. 120 (1998) 9714–9715;
b) T. Noda, H. Ogawa, Y. Shirota, Adv. Mater. 11 (1999) 283–285;
c) H. Doi, M. Kinoshita, K. Okumoto, Y. Shirota, Chem. Mater. 15 (2003) 1080–1089.
- a) S. Yamaguchi, S. Akiyama, K. Tamao, J. Am. Chem. Soc. 122 (2000) 6335–6336;
b) S. Yamaguchi, S. Akiyama, K. Tamao, J. Am. Chem. Soc. 123 (2001) 11372–11375;
c) Z. Zhou, A. Wakamiya, T. Kushida, S. Yamaguchi, J. Am. Chem. Soc. 134 (2012) 4529–4532;
d) M. Steeger, C. Lambert, Chem. Eur. J. 18 (2012) 11937–11948.
- a) W.L. Jia, X.D. Feng, D.R. Bai, Z.H. Lu, S. Wang, G. Vamvounis, Chem. Mater. 17 (2005) 164–170;
b) W.L. Jia, M.J. Moran, Y. Yan Yuan, Z.H. Lub, S. Wang, J. Mater. Chem. 15 (2005) 3326–3333;
c) X.Y. Liu, D.R. Bai, S. Wang, Angew. Chem. Int. Ed. 45 (2006) 5475–5478;
d) Z. Zhang, R.M. Edkins, J. Nitsch, K. Fucke, A. Eichhorn, A. Steffen, Y. Wang, T.B. Marder, Chem. Eur. J. 21 (2015) 177–190.
- a) S. Yamaguchi, T. Shirasaka, K. Tamao, Org. Lett. 2 (2000) 4129–4132;
b) E. Sakuda, Y. Ando, A. Ito, N. Kitamura, J. Phys. Chem. A 114 (2010) 9144–9150.
- a) J.J. Peterson, M. Werre, M.Y.C. Simon, E.B. Coughlin, K.R. Carter, Macromolecules 42 (2009) 8594–8598;
b) K. Kokado, A. Nagai, Y. Chujo, Macromolecules 43 (2010) 6463–6468;
c) B.P. Dash, R. Satapathy, E.R. Gaillard, K.M. Norton, J.A. Maguire, N. Chug, N.S. Hosmane, Inorg. Chem. 50 (2011) 5485–5493;
d) K.R. Wee, W.S. Han, D.W. Cho, S. Kwon, C. Pac, S.O. Kang, Angew. Chem. Int. Ed. 51 (2012) 2677–2680.
- a) J.O. Huh, H. Kim, K.M. Lee, Y.S. Lee, Y. Do, M.H. Lee, Chem. Commun. 46 (2010) 1138–1140;
b) K.M. Lee, J.O. Huh, T. Kim, Y. Do, M.H. Lee, Dalton Trans. 40 (2011) 11758–11764.
- M.J. Mio, L.C. Kopel, J.B. Braun, T.J. Kadzikwa, K.L. Hull, R.G. Brisbois, Org. Lett. 4 (2002) 3199–3202.
- SMART and SAINT, Bruker Analytical X-Ray Division, 2002. Madison, WI.
- G.M. Sheldrick, SHELXTL-PLUS Software Package, Bruker Analytical X-Ray Division, 2002. Madison, WI.
- M.J. Frisch, et al., Gaussian 09, Revision D.01, Gaussian Inc., Wallingford, CT, 2013.
- M.G. Davidson, T.G. Hibbert, J.A.K. Howard, A. Mackinnon, K. Wade, Chem. Commun. (1996) 2285–2286.
- M.A. Fox, C. Nervi, A. Crivello, P.J. Low, Chem. Commun. (2007) 2372–2374.
- A. Ito, K. Kawanishi, E. Sakuda, N. Kitamura, Chem. Eur. J. 20 (2014) 3940–3953.
- a) N. Mataga, Y. Kaifu, M. Koizumi, Bull. Chem. Soc. Jpn. 29 (1956) 465–470;
b) V.E.Z. Lippert, Elektrochem 61 (1957) 962–975.